Radio Science, Volume ???, Number , Pages 1–23,

Improving GNSS-R sea level determination through inverse modeling of SNR data

Joakim Strandberg[1], Thomas Hobiger[1] and Rüdiger Haas[1]

[1]Department of Earth and Space Sciences,

Chalmers University of Technology,

Gothenburg, Sweden

Key Points.

- We present an advanced method for retrieving sea-surface heights using inverse modeling of SNR observations.
- The new method models sea-surface heights as a continuous function using B-splines.
- Data from several GNSS signals are seamlessly combined for increased precision.

This paper presents a new method for retrieving sea-surface heights from GNSS-R data by inverse modeling of SNR observations from a single geodetic receiver. The method relies on a B-spline representation of the temporal sea level variations in order to account for its continuity. The corresponding B-spline coefficients are determined through a non-linear least-squares fit to the SNR data, and a consistent choice of model parameters enables the combination of multiple GNSS in a single inversion process. This leads to a clear increase in precision of the sea level retrievals which can be attributed to a better spatial and temporal sampling of the reflecting surface. Tests with data from two different coastal GNSS sites and comparison with co-located tide gauges show a significant increase in precision when compared to previously used methods, reaching standard deviations of 1.4 cm at Onsala, Sweden, and 3.1 cm at Spring Bay, Tasmania

1. Introduction

Since it was demonstrated that reflected GNSS signals can be used to monitor local sea-surface heights [*Soulat et al.*, 2004], the concept has been attractive as it is relatively inexpensive and easy to deploy and operate. Furthermore, the GNSS technology can relate the sea level measurements to a global reference frame, which means that GNSS reflectometry (GNSS-R) can directly distinguish between relative and absolute sea-surface change, something traditional tide gauges cannot do without additional equipment.

Various concepts exist for GNSS-R, and they can be broadly categorized into two groups – phase difference analysis [*Soulat et al.*, 2004; *Löfgren et al.*, 2011] and signal-to-noise ratio (SNR) analysis [*Larson et al.*, 2013]. The first technique uses two antennas to determine the difference in phase between the direct and the reflected signal, and thereby their path length difference. The latter uses only a single antenna, instead analyzing the SNR pattern from the GNSS satellites to determine the sea-surface height. A benefit of using the SNR method is greater robustness to wind and wave conditions [*Löfgren and Haas*, 2014], and it has also been demonstrated that the method is useful for determining other important sea-state parameters, such as significant wave height [*Alonso-Arroyo et al.*, 2015]. However the method has so far been less precise than the phase difference analysis. Therefore, this paper presents a new algorithm for retrieving sea-surface heights from GNSS SNR data, that increases the precision of single receiver GNSS tide gauges.

2. GNSS-R and sea level

The recorded SNR at a ground-based GNSS station varies during a GNSS satellite passage. In general, the SNR depends on different factors such as satellite signal strength, antenna gain pattern, and multipath environment. According to *Nievinski and Larson* [2014b], in case of a single multipath reflection, SNR (in watt/watt) can be written as

$$\mathrm{SNR} = P_d \left(1 + P_i + 2\sqrt{P_i}\cos(\phi_i)\right)/P_n + P_s^I/P_n. \tag{1}$$

Here, P_d is the power received directly from the satellite, P_i is the relative interferometric power due to reflections, P_s^I is the incoherent signal power, and P_n is the noise power. Assuming a horizontal reflecting surface, the interferometric phase ϕ_i can be written as

$$\phi_i = \frac{4\pi h}{\lambda}\sin(\varepsilon) + \varphi. \tag{2}$$

Here, h is the reflector height, i.e. the vertical distance from the phase center of the GNSS antenna to the reflecting surface, ε is the elevation angle of the satellite, and λ its signal wavelength, while φ contains the phase contribution of the antenna pattern and electromagnetic properties of the reflecting surface.

Focusing on the geometry-dependent part, SNR observations are usually divided into a trend, tSNR, which mainly depends on the satellite elevation, and the oscillating part δSNR:

$$t\mathrm{SNR} = P_d\left(1 + P_i\right)/P_n + P_s^I/P_n, \tag{3}$$

$$\delta\mathrm{SNR} = 2P_d\sqrt{P_i}\cos(\phi_i)/P_n. \tag{4}$$

Previous studies, for example by *Larson et al.* [2013], have focused on the interferometric phase ϕ_i for retrieving sea-surface heights through spectral analysis of δSNR. Following these studies, if we write δSNR as a function of $x = \sin(\varepsilon)$by inserting the interferometric phase of Eq. (2) into Eq. (4), and then neglect the elevation dependency of P_d, P_i and φ, we obtain

$$\delta\mathrm{SNR} = A\cos\left(\frac{4\pi h}{\lambda}x + \varphi\right), \tag{5}$$

where $A = 2P_d\sqrt{P_i}/P_n$ becomes a constant factor. Therefore, the main spectral component can be translated into a distance between the antenna and the sea surface.

However, the spectral method ignores effects of temporal reflector height variations. This is acceptable for coastal sites with small tidal range, where the water level is relatively stationary during a satellite pass. But for sites with large sea level variations a correction term must be added, for example based on tidal models [*Löfgren and Haas*, 2014]. *Roussel et al.* [2015] instead introduced a method based on the Lomb-Scargle inversion that combines all available GNSS signals, by fitting h and $\frac{\mathrm{d}h}{\mathrm{d}t}$to all satellites visible during a measurement time span. However, their study considers only a correction term for linear temporal changes of the reflector height. In contrast to this, we present here an advanced method that directly accounts for temporal changes in sea-surface heights, by modeling height as a smooth function.

3. Advanced sea-surface height retrieval by inverse modeling

In the present study we use inverse modeling, i.e. we fit an analytic function to measured δSNR oscillations. Thus, we do not rely on spectral methods, but use a

physical model for the data analysis. Similar methods have previously been used for snow depth estimation [*Nievinski and Larson*, 2014c], where single satellite arcs were analyzed independently, assuming a static reflector height. In order to benefit from the sophisticated properties of inverse modeling, and considering that sea-surface height variations can be approximated as a smooth process, we present an advanced method for sea-surface height retrieval hereafter.

First, we extend the simplified form of Equation (5) with an attenuation factor in order to account for the decrease of the multipath oscillation amplitude with increasing elevation. The attenuation factor

$$S^2 = \mathrm{e}^{-4k^2 s^2 \sin^2(\varepsilon)} \tag{6}$$

relates to the interferometric power P_i of Equation (4), where k is the wave number, and s is the standard deviation of the reflector surface height. This term accounts for loss of coherence in the reflected signal due to surface random roughness [*Beckmann and Spizzichino*, 1963].

The oscillating part of the SNR will therefore be modeled as:

$$\delta\mathrm{SNR} = \left(C_1 \sin\left(\frac{4\pi h}{\lambda} x\right) + C_2 \cos\left(\frac{4\pi h}{\lambda} x\right) \right) \mathrm{e}^{-4k^2 \Lambda x^2}, \tag{7}$$

where in-phase/out-of-phase terms C_1 and C_2 replace amplitude and phase in Equation (5) for numerical stability during the inversion process. The term $\Lambda = s^2$ is introduced for the same reason.

Conversion back to A and φ is achieved by the following basic relations:

$$A = \sqrt{C_1^2 + C_2^2}, \tag{8}$$

and

$$\varphi = \tan^{-1}(C_2/C_1). \tag{9}$$

Now Eq. (7) combines geometric and radiometric information and represents a well-suited functional model that enables sea-surface height retrievals from the inversion of SNR data.

As discussed in the previous section, only δSNR is of interest for determining the sea-surface height. Therefore, only SNR-measurements from directions towards open water are converted to linear scale (i.e. watt/watt), and then detrended using a low order polynomial. This ensures that signatures originating from antenna gain pattern and other factors are removed to a large extent, and that the observable of interest, δSNR, becomes accessible for further data analysis. By using a non-linear least-squares algorithm (cf. Section 3.2), an analytic model is fit to the remaining oscillations, as shown in Figure 1.

For a particular coastal site one can assume that the amplitude, phase, and damping factors are constants or slowly varying in time, while sea-surface height usually varies more rapidly. According to *Nievinski and Larson* [2014a], the amplitude is mainly influenced by satellite signal strength, receiver characteristics, and electromagnetic properties of the reflecting surface. These influencing factors can in general be assumed to be constant over a few days. The phase φ is also dependent on the electromagnetic properties of the reflecting surface, enabling us to treat it as constant over a few days. However, treating φ as a constant neglects non-geometric elevation dependence of the phase, for example from reflections and antenna patterns which

can lead to a bias in the retrieved reflector heights [*Nievinski*, 2013]. Correct modeling of such effects would therefore further increase the precision of the algorithm. The damping relates to surface random roughness, which is driven by average local wind speed and direction, and the shape of the coastline. In a first-order approximation we can also assume the damping to be constant over a few days. It is however important to notice that unless antenna characteristics are modeled properly, the $\Lambda = s^2$ parameter will not only include information from the surface roughness, but also from the antenna gain pattern. Therefore, care should be taken when interpreting the values of this parameter. Modeling these properties as constants allows us to combine data from several GNSS satellites, and even different systems, via the information implicitly shared through common parameters.

For the coastal sites tested in this work, cf. Section 4, this means that SNR measurements from both GPS and GLONASS satellites, and the L1 and L2 frequency of both systems, are used in a consistent inversion process. To consider varying signal strengths and frequency dependent reflection phase offsets, both A and φ, i.e. C_1 and C_2, are estimated per satellite system and wavelength, i.e. one set for GPS L1, one for GLONASS L1, etc. The roughness parameter s is however not dependent on the signal, but rather on geometric properties of the reflector, and thus is considered as a single constant parameter. Sea-surface height information is also shared across all the satellite systems and wavelengths. However, the sea-surface height undergoes significant temporal changes. In order to handle this temporal variation we introduce

a B-spline representation for the sea-surface height, which is described in the next section.

3.1. Modeling sea-surface heights by B-Spline functions

As discussed before, SNR interference patterns contain the necessary information to obtain geometric and radiometric properties of the reflecting surface. Although arc-wise inversion, for example by spectral methods [*Larson et al.*, 2013], has been proven to be a powerful GNSS-R approach, it does not make use of the knowledge that the estimated parameters are continuous. In particular for GNSS-R sea level applications, we assume that the sea surface varies as a smooth function which should therefore be included in the retrieval process.

In principle, any analytic function that considers tidal and long-term variations is sufficient to be implemented in a straightforward inversion algorithm. Piece-wise linear models might be the simplest functional approach but lead to discontinuities at the nodes when computing first-order derivatives. As already discussed by *Hobiger et al.* [2014] and *Hobiger et al.* [2016], B-spline functions can help to overcome such deficits while still providing enough variability to consider the most dominant sub-daily and long-term sea level variations. In their basic form, B-spline functions are constructed from zero-degree basis functions which are defined as

$$N_j^0(t) = \begin{cases} 1 & \text{if } t_j \leq t < t_{j+1} \\ 0 & \text{otherwise} \end{cases} , \tag{10}$$

and B-spline basis functions of higher order r can be recursively computed by the relation

$$N_j^r(t) = \frac{t - t_j}{t_{j+r} - t_j} N_j^{r-1}(t) + \frac{t_{j+r+1} - t}{t_{j+r+1} - t_{j+1}} N_{j+1}^{r-1}(t). \quad (11)$$

With these basis functions sea-surface height variations can be approximated as

$$h(t) = \sum_{j=0}^{N} h_j N_j^r(t) \quad (12)$$

when node values $h_0, ..., h_N$ are estimated from the SNR data. Herein, $N+1$ denotes the total number of nodes. For most applications, quadratic or cubic B-spline functions are chosen to approximate signals that are expected to be continuous in the first- or second-order derivatives. The capability of resolving certain spectral features depends only on the temporal spacing of the nodes, which means that one can place more nodes when expecting higher frequency components or increase the temporal node spacing when dealing with rather low-frequent signals. In this study, quadratic B-spline functions $N_j^2(t)$ are used as the sea-surface height is assumed to be a smooth function.

An important feature of B-spline functions is that they are obtained as a linear combination of the basis functions and node values as denoted in Eq. 12. Therefore it is straightforward to evaluate the continuous function at any given epoch while only dealing with a relatively small number of coefficients. Moreover, the linearity of Eq. 12 makes it easy to estimate the coefficients by least-squares methods.

3.2. Non-linear least-squares parameter estimation

Considering that amplitudes $C_{1,i}$ and $C_{2,i}$, and the damping factor Λ are estimated as constants over the time span considered in the data analysis, the total number of parameters M_T which needs to be estimated from a consistent inverse modeling is

$$M_T = M_B + 2 \cdot M_f + 1, \tag{13}$$

where M_B denotes the number of B-spline nodes and M_f is the number of GNSS frequencies which are used. Even with moderate sampling rates, e.g. a 30 s sampling interval, and a dense choice of B-spline nodes, e.g. one per hour, it is obvious that the number of observations is much larger than the number of unknowns which should be estimated. Therefore, one faces an over-determined parameter estimation problem, which would be normally solved by least-squares adjustment, i.e. finding an optimum set of parameters $x_0, x_1, \ldots, x_{M_T}$, that minimizes the cost function

$$\min \sum_N \left(y_i - f(x_0, x_1, \ldots, x_{M_T})\right)^2, \tag{14}$$

where N is the total number of observations and y_i are SNR measurements. However, the high non-linearity of the functional model (cf. Equation (7)) does not allow for a classical least-squares solution. Instead, a non-linear least-squares method needs to be applied. The MINPACK libraries [*Moré et al.*, 1980], which are interfaced via the "optim" package within the Python framework SciPy [*Oliphant*, 20107; *Millman and Aivazis*, 2011], provide a convenient solution and easy-to-use environment which has been used in this work. Thus, inverse modeling of SNR interference patterns becomes possible even when the relation between the model parameters and the observed SNR variations is highly non-linear.

3.3. Parametrization and initial conditions

In order to retrieve sea-surface heights it is important that the analyzed SNR patterns come from reflections off the water surface. To ensure that only relevant reflections from water are analyzed only directions where the characteristic oscillating pattern is observed are considered in the analysis process. The process is further described in [*Löfgren et al.*, 2014]. This results in station specific azimuth/elevation sectors in which water reflections are expected.

The choice of initial parameters in the non-linear least-squares estimation process is crucial. Especially the initial distance between the antenna and the sea surface is of importance, since it determines whether the solver converges to the global or a local minimum. Therefore, the initial height should be chosen site-specific, using a representative value for the average antenna height above the sea level, setting all a priori B-spline node values to this initial estimate. The other parameters, C_1, C_2, and Λ, are less sensitive to their a priori values, and do not need to be initialized site-specific.

Another point of interest is the number of nodes used for the B-spline implementation, as it determines the maximum temporal resolution of the solution. For a high temporal resolution a large number of nodes is desirable, however this will increase the computational load of the non-linear least-squares estimation and may eventually degrade the final solution due to overfitting. Furthermore, the SNR data are not continuous, and there are data gaps when no satellites are within the azimuth/elevation sectors considered in the analysis process. These periods without data impose a limit

on the temporal resolution of the inversion process, since all B-spline intervals must cover a time span with sufficient data. Thus the B-spline intervals must be larger than the longest gaps in the data set.

The B-spline solution can occasionally be unstable at the beginning or the end, especially if there are data gaps. Therefore, we perform an inversion process with data from three consecutive days, but select only the results of the middle day. This processing scheme is applied to each day in order to obtain a smooth and continuous time series of sea-surface heights.

4. Testing and validating the method at two coastal sites

The new method has been tested with data from the GNSS stations at Onsala (GTGU) at the Swedish west coast, and Spring Bay (SPBY) at the east coast of Tasmania, cf. Section 4.1 and 4.2. Both stations are located on the coast and have a good view of open water. In addition, the two installations record SNR data from both GPS and GLONASS with high temporal resolution. Moreover, both stations are co-located to tide gauges for independent validation and have been previously used for GNSS-R related studies.

4.1. Onsala GNSS-R installation (GTGU)

The GNSS-R tide gauge at the Onsala Space Observatory was installed in the fall of 2011, and has been previously described by *Larson et al.* [2013]. The site was installed specifically for GNSS-R purposes and therefore has a wide view over the sea, covering almost 180 degrees in azimuth (c.f. Table 1 for azimuth/elevation ranges).

The equipment at the site includes two Leica AR 25 GNSS antennas, one zenith and one nadir looking. The nadir looking antenna is modified to be sensitive for left-hand circularly polarized signals. Both antennas are mounted on a horizontal pole which allows them to be placed up to 4 m above the mean sea level. Each antenna is connected to a separate Leica GRX1200 receiver. Thus it is possible to use the up-ward looking installation (called GTGU) for GNSS-R studies using SNR data or investigate sea-surface height changes by utilizing the phase difference between the up-ward and down-ward looking antenna/receiver pairs. During the period studied in Sec. 5, data from a co-located pressure tide gauge with a nominal uncertainty of 5 mm were available. As this tide gauge is only 10 m away from the GNSS-R station, it can be used as a reference to which GNSS-R solutions can be compared to.

In general, it can be stated that the tidal variations at Onsala are relatively small, and have a daily peak-to-peak variation of around 20 cm. However, meteorological effects, in particular local pressure variations that influence the sea level, are the primary driver for sea level variations at the site. These effects lead to a maximum peak-to-peak variation of the sea-surface height of around 80 cm over the test period.

4.2. Spring Bay GNSS-R installation (SPBY)

The Spring Bay GNSS-R installation is situated close to the city Spring Bay in Tasmania, Australia, and is operated by Geoscience Australia. The site was not installed for GNSS-R purposes, but rather for position monitoring, and has a smaller acceptable azimuth/elevation range than GTGU, see Table 1. Since the equipment at the site only consist of one single zenith looking Leica AT504 GG antenna, only

SNR analysis is possible at the site. The antenna is mounted approximately 4 m above the average sea surface and is connected to a Leica GRX1200 receiver.

There is a co-located acoustic tide gauge at the site which gives one measurement each minute. These measurements are computed as averages from 1 Hz data over a period of one minute. The standard deviation during one minute is on average 1.3 cm for the time period studied in this paper.

The peak-to-peak variation of the daily tides at Spring Bay is larger than at Onsala and are approximately 80 cm. Together with long periodic effects, the total peak-to-peak variation was around 1.3 m during the test period.

5. Results

To compare with earlier studies at the Onsala GNSS-R tide gauge, cf. Section 4.1, the new algorithm, cf. Section 3, was tested with data from 2012, day of year (doy) 273 to 303. These data were previously analyzed by *Löfgren and Haas* [2014] with both the Lomb-Scargle algorithm, with height rate corrections, as well as with the phase difference method. The authors report standard deviations for the difference when comparing to a co-located pressure tide gauge of 4.0 cm and 3.2 cm respectively.

In this work, the retrieved sea-surface heights are represented as B-spline functions. Therefore, to compare with measurements from a co-located pressure tide gauge, the B-spline representations are evaluated at the epochs of the pressure tide gauge measurements. For GTGU the standard deviation becomes 1.4 cm, which is a significant

improvement in precision not only in respect with the previously used SNR method, but also in comparison with the phase difference analysis.

The inverse modeling method was also compared with the Lomb-Scargle spectral method on data from the GNSS station SPBY in Spring Bay, Australia. The time period for the tests on this site was stipulated by the presence of a continuous series of data with high temporal resolution, and was chosen to be between doy 283 and 324, 2015.

In Figure 4 the standard deviation, with respect to the co-located tide gauge, for the full period is presented for both the inverse-modeling method presented in this paper, and the Lomb-Scargle spectral method. As the site only has one upward-looking antenna the phase difference method is unfeasible, and only the performance of the two SNR-methods can be evaluated. The standard deviation between the sea-surface heights retrieved by inverse-modeling and the co-located tide gauge is 3.1 cm for the whole period. In comparison, the best value for the Lomb-Scargle analysis on this data set, which is from the L1 signal from GLONASS satellites, yields a standard deviation of 9.8 cm, which is similar to the results presented by *Santamaría-Gómez et al.* [2015], where the lowest standard deviation for the whole year of 2013 was found to be 8.5 cm.

As seen from Table 2 and Figure 4, the capability to simultaneously process data from multiple GNSS is beneficial, as the combination of GPS and GLONASS leads to higher precision than using them separately. However, combining L1 and L2 signals in a single inversion process did not result in a significantly improved precision. This

shows that it is not the increased amount of data points available in the inversion process that is the origin of the improvement, but rather the improved temporal and spatial coverage that using several GNSS together provides. More satellites means a higher probability that a GNSS surface reflection is available within the accepted azimuth/elevation sectors at any given time.

The standard deviation of the two stations for different numbers of B-spline nodes are presented in Figure 5. As expected, a higher temporal resolution at first increases the precision of the algorithm. However, after a certain threshold, the precision starts to deteriorate. Such deterioration is a general problem when fitting functions, also known as overfitting. This threshold occurs at a higher number of B-spline nodes for GTGU, which has larger azimuth/elevation sectors, than for SPBY. A wider angle mask means more SNR measurements and less, and shorter, gaps where no data at all are available. This also implies that a higher temporal resolution of the B-spline model becomes feasible without the risk of overfitting.

The sharp increase in standard deviation that occurs at lower number of nodes at SPBY arises since the small number of B-spline nodes reduces the ability to resolve the semi-diurnal tides that are dominant at Spring Bay. For GTGU the same increase in standard deviation is not observed as semi-diurnal tides are less important at Onsala than meteorological effects, which dominate the local sea level and occur on longer timescales.

As discussed before, it can be stated that the new inverse modeling strategy outperforms both the Lomb-Scargle and phase-difference methods in terms of smaller

standard deviation. Moreover, as shown in Table 2, higher correlations against measurements from a co-located tide gauge are obtained when using the inverse modeling approach. Since tides are periodic by nature it is possible to study more than simple correlations and investigate how well the tide gauge records and the retrieved heights from both the inverse modeling algorithm and the Lomb-Scargle method agree on different time scales. This is done with wavelet coherence analysis using a MATLAB-implementation based on the work by *Grinsted et al.* [2004]. The coherence between the sea-surface heights retrieved from GNSS-R and the tide gauges are shown in Figures 6 and 7, for GTGU and SPBY respectively. Since the wavelet analysis requires a regularly sampled signal, the heights derived from the Lomb-Scargle analysis are re-sampled using linear interpolation. As this might affect the coherence on periods shorter than the original spacing of the data, only time scales above the longest time between two successive Lomb-Scargle solutions are considered here.

From Figures 6 and 7 it is clear that the coherence for the inverse modeling is in general higher than for the Lomb-Scargle solution. In particular, the inverse modeling coherence is preserved for periods down to 6 h, whereas the Lomb-Scargle approach is only capable to resolve spectral components with periods of 8 h or longer. Over all, inverse modeling outperforms the Lomb-Scargle results in terms of coherence on all time scales.

Although not discussed here, an analysis of the post-fit residuals revealed no systematic effects or signals, which confirms that the chosen parameterization is suitable

to model the data. Thus, the presented inversion strategy appears to a good choice for retrieving sea-surface heights from GNSS SNR data.

6. Conclusion and outlook

The precision of interferometric GNSS-R analysis has been increased by using a new algorithm for retrieving sea-surface heights from GNSS SNR data, based on inverse modeling of SNR observations. Tests at two different sites confirm this increase in precision when comparing against the Lomb-Scargle method and the dual receiver method applied to GTGU data.

The precision of the inversion increased when signals from GPS and GLONASS were consistently combined. However, combining data from L1 and L2 signals did not improve precision. Both findings can be explained by the fact that better geometric coverage tends to improve the inversion whereas more data from the same time and location do not lead to significantly better sea level retrievals. Therefore, adding data from more GNSS as they become available has the potential to increase the precision of our algorithm, since more available satellites lead to a higher probability for a satellite to be within the accepted azimuth/elevation ranges at any given time.

However, even using only one of the signals, the method increases the precision significantly compared to previously used methods. This paves the way for using low-cost GNSS equipment for precise sea level studies.

The number of B-spline nodes used in the inversion model has a significant impact on the precision of the solution. However, the optimum number of nodes can only

be determined with knowledge about local sea visibility conditions, as well as tidal variations at a particular site. Further studies will show how to automatically adopt the algorithm for an arbitrary coastal site.

Acknowledgments. The International GNSS Service [*Dow et al.*, 2009] is acknowledged for providing data and products. The SPBY GNSS data are freely available and distributed by Geosciences Australia. Data from the Spring Bay tide gauge are distributed upon request by the Australian Bureau of Meteorology. The GNSS equipment (receivers and antennas) at Onsala were funded by the Adlerbertska Foundation and purchased through the Leica Geosystems ATHENA program.

References

Alonso-Arroyo, A., A. Camps, P. Hyuk, D. Pascual, R., Onrubia, and F. Martin (2015), Retrieval of significant wave height and mean sea surface level using the GNSS-R interference pattern technique: results from a three-month field campaign, *EEE Trans. Geosci. Remote Sens.*, *53*(6), 3198–3209.

Beckmann, P., and A. Spizzichino (1963), *The scattering of electromagnetic waves from rough surfaces*, Pergamon Press (Republished by Artech House 1987).

Dow, J.M., R. E. Neilan, and C. Rizos (2009), The international GNSS service in a changing landscape of global navigation satellite systems, *Journal of Geodesy*, *83*(3), 191–198.

Grinsted, A., J. C. Moore, and S. Jevrejeva (2004), Application of the cross wavelet transform and wavelet coherence to geophysical time series, *Nonlinear processes in*

geophysics, *11*(5/6), 561–566.

Hobiger, T., R. Haas, and J. Löfgren (2014), GLONASS-R: GNSS reflectometry with a Frequency Division Multiple Access-based satellite navigation system, *Radio Science*, *49*(4), 271–282.

Hobiger, T., R. Haas, and J. Löfgren (2016), Software-Defined Radio Direct Correlation GNSS Reflectometry by Means of GLONASS, *IEEE Journal of Selected Topics in Applied Earth Observations and Remote Sensing*, in print.

Larson, K.M., J. S. Löfgren, and R. Haas (2013), Coastal sea level measurements using a single geodetic GPS receiver, *Advances in Space Research*, *51*(8), 1301–1310.

Löfgren, J. S., R. Haas, H.G. Scherneck, and M. Bos (2011), Three months of local sea level derived from reflected GNSS signals, *Radio Science*, *46*(6)

Löfgren, J. S., R. Haas, and H-G. Scherneck (2014), Sea level time series and ocean tide analysis from multipath signals at five GPS sites in different parts of the world, *Journal of Geodynamics*, *80*, 66–80

Löfgren, J. S., and R. Haas (2014), Sea level measurements using multi-frequency GPS and GLONASS observations, *EURASIP Journal on Advances in Signal Processing*, *2014*(1), 1–13.

Millman, K., and M. Aivazis (2011), Python for scientists and engineers, *Computing in Science & Engineering*, *13*(2), 9–12.

Moré, J. J., B. S. Garbow, and K. E. Hillstrom (1980), User Guide for MINPACK-1, *ANL-80-74*, 1980.

Nievinski, F. G. (2013), *Forward and inverse modeling of GPS multipath for snow monitoring* (Doctoral dissertation, University of Colorado, USA).

Nievinski, F. G., and K. M. Larson (2014a), Forward modeling of GPS multipath for near-surface reflectometry and positioning applications, *GPS solutions*, *18*(2), 309–322.

Nievinski, F. G., and K. M. Larson (2014b), Inverse modeling of GPS multipath for snow depth estimation–Part I: formulation and simulations, *IEEE Transactions on Geoscience and Remote Sensing*, *52*(10), 6555–6563.

Nievinski, F. G., and K. M. Larson (2014c), Inverse modeling of GPS multipath for snow depth estimation–Part II: application and validation, *IEEE Transactions on Geoscience and Remote Sensing*, *52*(10), 6564–6573.

Oliphant, T., (2007), Python for scientific computing, *Computing in Science & Engineering*, *9*(3), 10–20.

Roussel, N., G. Ramillien, F. Frappart, J. Darrozes, A. Gay, R. Biancale, N. Striebig, V. Hanquiez, X. Bertin, and D. Allain (2015), Sea level monitoring and sea state estimate using a single geodetic receiver, *Remote Sensing of Environment*, *171*, 261–258.

Santamaría-Gómez, A., C. Christopher, M. Gravelle, M. King, and G. Wöppelmann (2015), Levelling co-located GNSS and tide gauge stations using GNSS reflectometry, *Journal of Geodesy*, *89*(3), 241–258.

Soulat, F., M. Caparrini, O. Germain, P. Lopez-Dekker, M. Taani, and G. Ruffini (2004), Sea state monitoring using coastal GNSS-R, *Geophysical Research Letters*,

424 *31*(21).

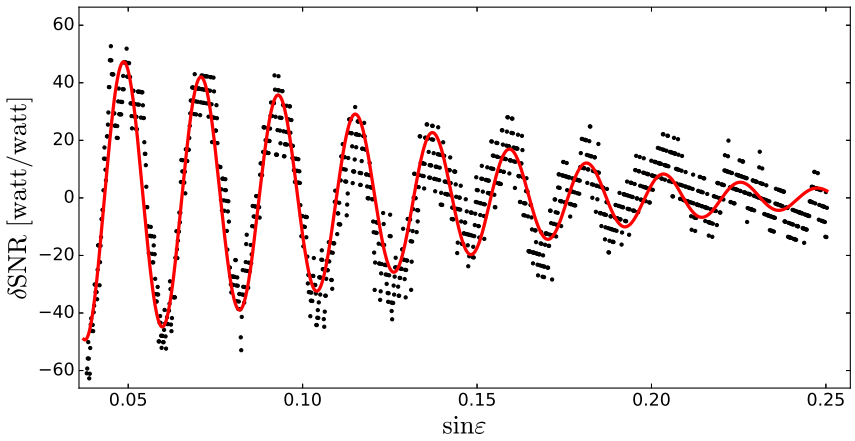

Figure 1. Detrended SNR from a GLONASS L1 arc (black dots) at GTGU on day 263, 2015, together with the SNR pattern obtained from inverse modeling (red line).

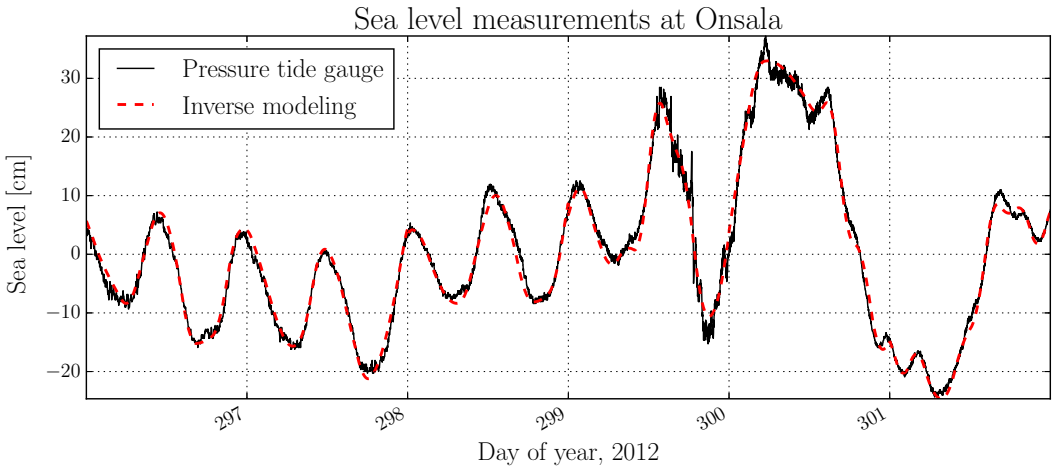

Figure 2. Sea level at Onsala as derived from inverse modeling of the detrended SNR data (red, dashed), and the reference levels from the co-located tide gauge (black, solid) for a subset of the data used for validation. Since the tide gauge and the GNSS solution do not have the same reference level, the mean of each of the two data sets has been removed before plotting.

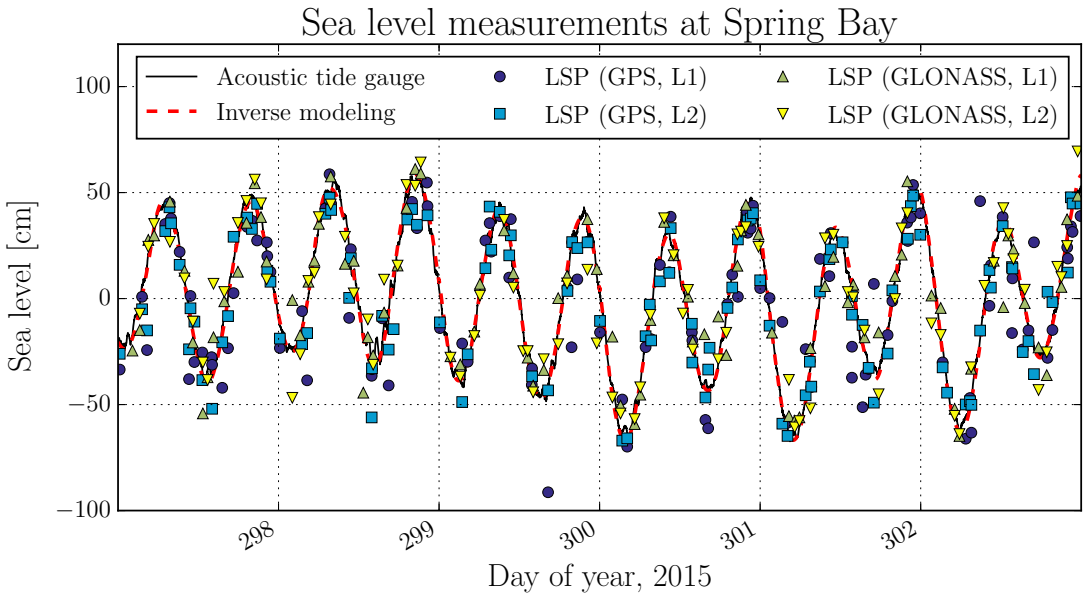

Figure 3. Results from pressure tide gauge (black, solid line), inverse modeling using both GLONASS and GPS (red, dashed line), and different Lomb-Scargle (LSP) solutions (symbols) for the GNSS station SPBY (Spring Bay, Australia). The mean of each data series has been removed before plotting.

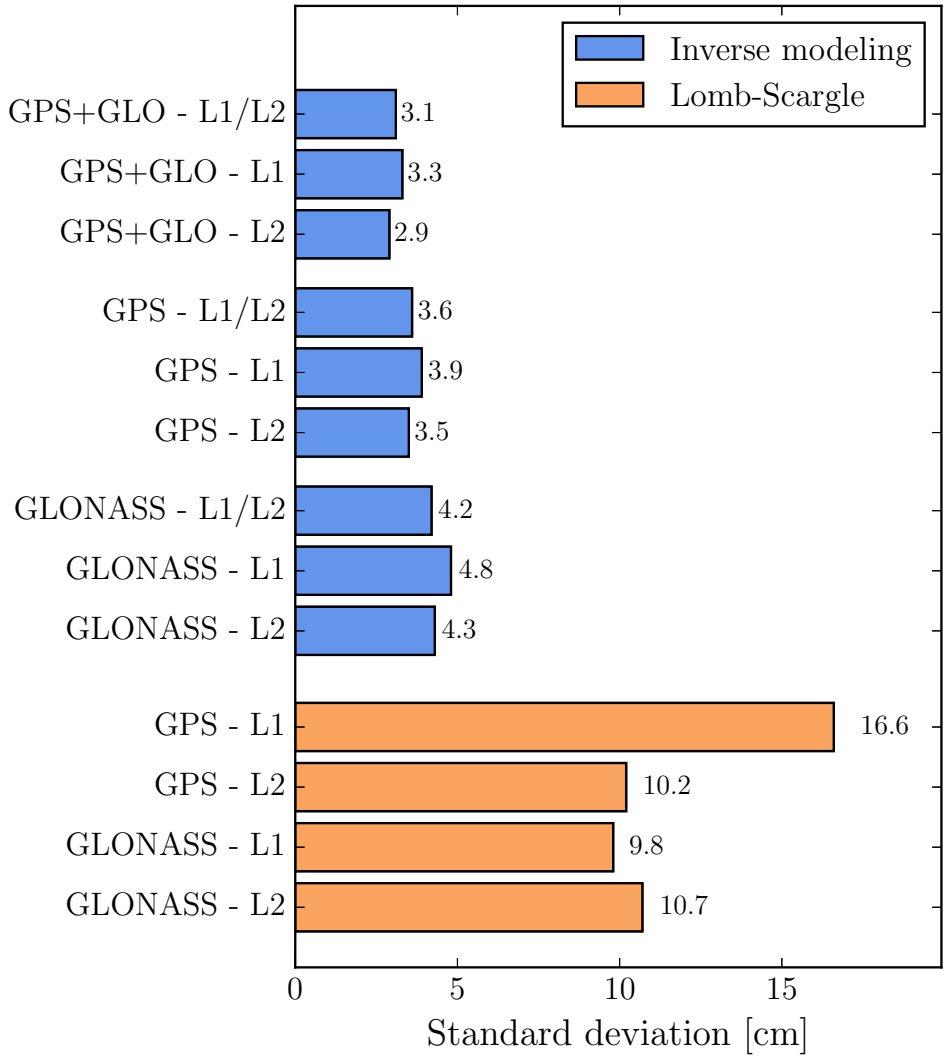

Figure 4. Standard deviation of the different GNSS-R sea level solutions w.r.t. the Spring Bay tide gauge for the full period from doy 283 to 324, 2015.

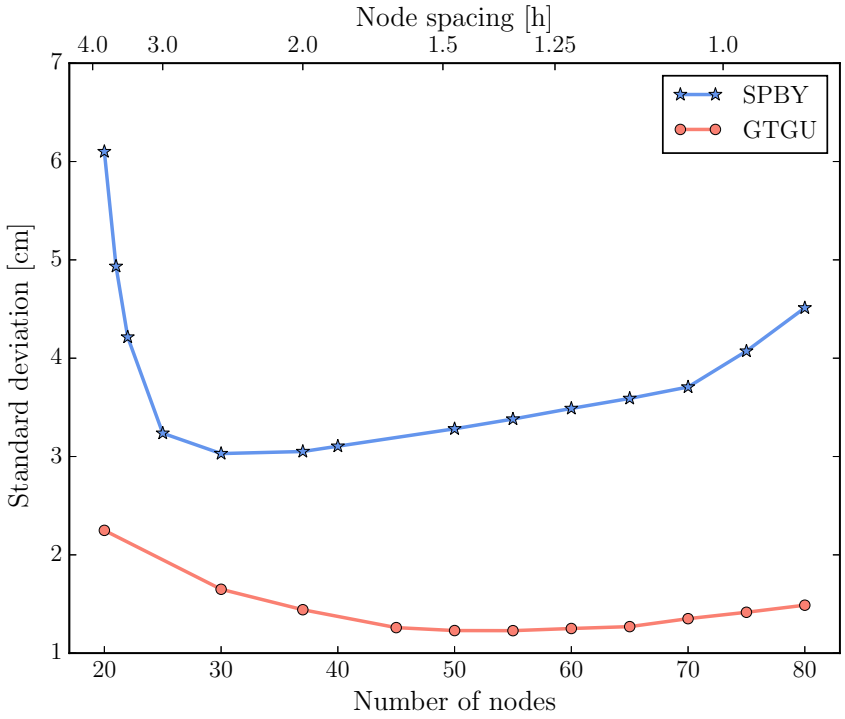

Figure 5. Standard deviations compared to co-located tide gauges for the GTGU and SPBY stations, using different number of B-spline nodes, and their spacing in time (upper axis), in the inverse modeling process.

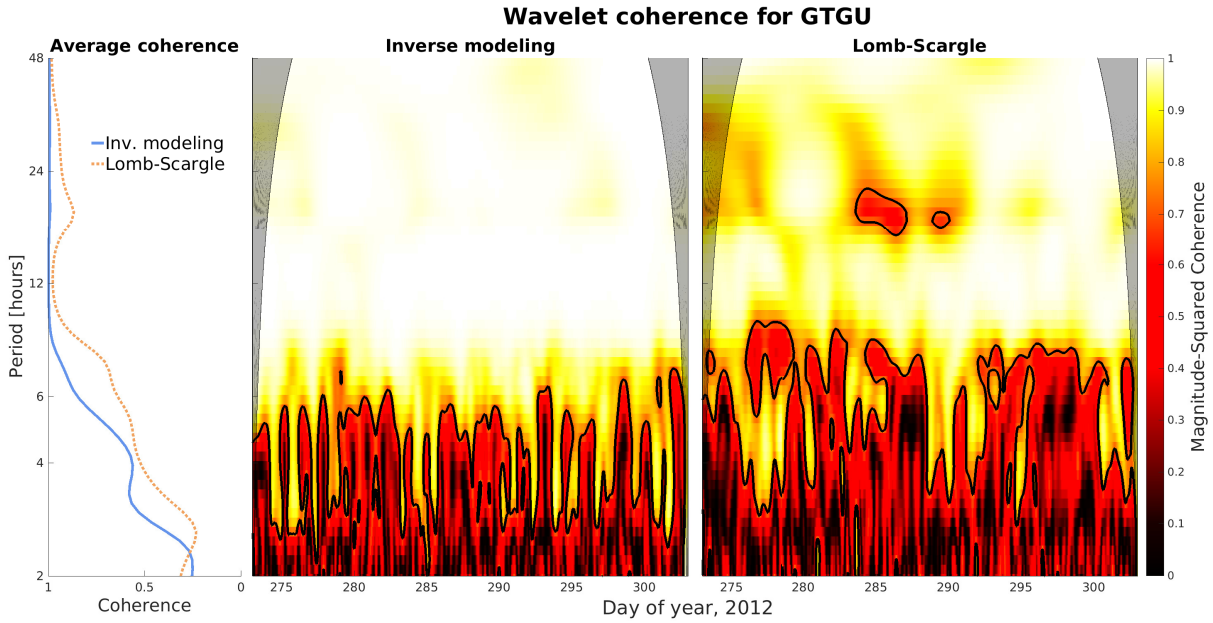

Figure 6. Wavelet coherence between the Onsala tide gauge measurements and the sea-surface heights retrieved by the inverse modeling (left) and the Lomb-Scargle method (right). The gray mask marks the areas where boundary effects impact the wavelet analysis, and the black contour marks the 5 % significance level against red noise.

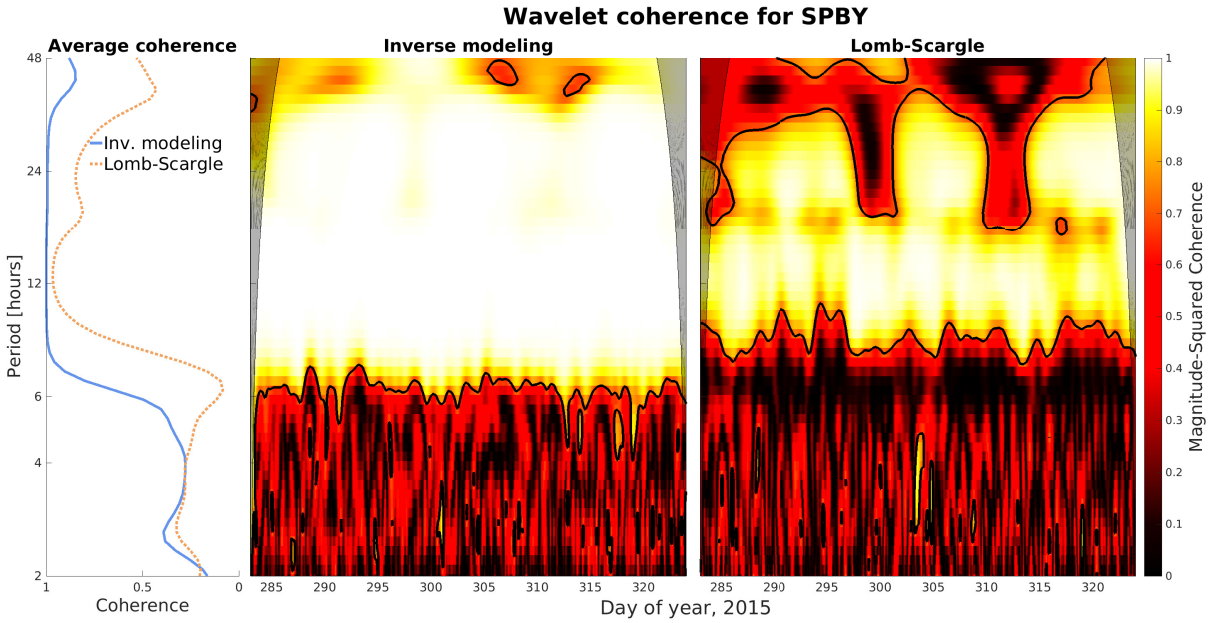

Figure 7. Wavelet coherence between the Spring Bay tide gauge measurements and the sea-surface heights retrieved by the inverse modeling (left) and the Lomb-Scargle method (right). The gray mask marks the areas where boundary effects impact the wavelet analysis, and the black contour marks the 5 % significance level against red noise.

Table 1. Azimuth/elevation ranges and initial heights for GTGU and SPBY

Station	Elevation range [deg]	Azimuth range [deg]	Initial height
GTGU	1 – 14.5	70 – 260	4 m
SPBY	1 – 10	280 – 310	4 m
	1 – 7	310 – 335	
	1 – 10	335 – 360	

Table 2. Comparison of different GNSS-R sea level solutions for GTGU, day of year 273 to 303, 2012

	Standard deviation [cm]	Mean abs. difference [cm]	Correlation
Inverse modeling			
GPS+GLO, L1/L2	1.44	1.13	0.99
GPS+GLO, L1	1.43	1.13	0.99
GPS+GLO, L2	2.00	1.58	0.99
GPS, L1/L2	1.54	1.21	0.99
GPS, L1	1.53	1.21	0.99
GPS, L2	2.32	1.84	0.99
GLONASS, L1/L2	1.68	1.33	0.99
GLONASS, L1	1.69	1.33	0.99
GLONASS, L2	2.24	1.77	0.99
Lomb-Scargle spectral analysis[a]			
GPS, L1	4.0	3.2	0.97
GPS, L2	9.0	7.5	0.86
GLONASS, L1	4.7	3.6	0.96
GLONASS, L2	8.9	7.0	0.87
Geodetic phase difference analysis[a]			
GPS, L1	3.5	2.3	0.95
GPS, L2	3.5	2.4	0.95
GLONASS, L1	3.3	2.2	0.96
GLONASS, L2	3.2	2.3	0.96

[a] Results from *Löfgren and Haas* (2014). Values only reported with mm resolution.